Isı Bilimi ve Tekniği Dergisi, 43, 1, 95-106, 2023
J. of Thermal Science and Technology
©2023 TIBTD Printed in Turkey
ISSN 1300-3615
https://doi.org/10.47480/isibted.1290741

# GEOMETRIC OPTIMIZATION OF A NANOSTRUCTURED W-$SiO_2$-W SELECTIVE EMITTER WITH TEMPERATURE DEPENDENT EMISSIVITY FOR THERMOPHOTOVOLTAIC APPLICATIONS

**Eslem Enis ATAK[a*], Elif Begüm ELÇİOĞLU[b**], Tuba OKUTUCU-ÖZYURT[c***]**
[a] Middle East Technical University, Department of Mechanical Engineering, 06800, Ankara, Turkey
[b] Eskişehir Technical University, Department of Mechanical Engineering, 26555 Eskişehir, Turkey
[c] İstanbul Technical University, Energy Institute, Renewable Energy Division, 34469, İstanbul, Turkey
* eatak@metu.edu.tr, ORCID: 0000-0002-6866-5207
** ebelcioglu@eskisehir.edu.tr, ORCID: 0000-0002-1005-4294
*** okutucuozyurt@itu.edu.tr, ORCID: 0000-0003-4248-8043

(Geliş Tarihi: 15.09.2022, Kabul Tarihi: 31.03.2023)

**Abstract:** Metal-Insulator-Metal (MIM) nanostructures provide tunable multiple absorption/emission peaks desirable for spectroscopy, light sensing and thermophotovoltaic (TPV) applications. The efficiency of TPV systems can be improved by employing MIM emitters with resonators that allow high emission above PV cell bandgap and low emission elsewhere. Although there have been attempts to design MIM emitters for TPV systems, a comprehensive study that investigates and optimizes different resonator shapes is lacking. In this study, broadband TPV emitters with W-$SiO_2$-W nanostructures are optimized for pairing with GaSb PV cells. A numerical approach is followed utilizing finite-difference time-domain method and particle swarm optimization scheme, MIM emitters with four resonator shapes: disk, square, pyramid, and cone are dimensionally optimized to attain an emissivity spectrum that overlaps with high quantum efficiency region of the GaSb cell. The optimized emitters are compared for efficiency, power output, material consumption, as well as their optical response to temperature and angular effects. At an emitter temperature of 1600 K, electrical power outputs of 2.335-2.418 $W \cdot cm^{-2}$ and spectral efficiencies of 56.2-57.6% are obtained. It is found that flat resonators tend to achieve similar performance to that of pointy resonators with shorter heights. Among the considered shapes, disk emitter demonstrates the highest efficiency with minimum material consumption. Compared to a plain W emitter at the same temperature, the disk MIM emitter exhibits significantly higher spectral efficiency and electrical power output (34% and 215% respectively). The results demonstrate the successful use of nano-elements in TPV systems, and the potential for fabricating and realizing such structures.
**Keywords:** Metal-insulator-metal, selective emitter, surface plasmon polariton, magnetic polariton, nanostructure, thermal radiation harvesting, particle swarm optimization.

# SICAKLIĞA BAĞLI YAYINIM GÖSTEREN NANOYAPILI W-$SiO_2$-W SEÇİCİ YAYICININ TERMOFOTOVOLTAİK UYGULAMALAR İÇİN GEOMETRİK OPTİMİZASYONU

**Özet:** Metal-yalıtkan-metal (MIM) nanoyapılar, ışık algılama, spektroskopi ve termofotovoltaik (TPV) uygulamalar için arzu edilen, ayarlanabilir soğurma/yayma spektrumu oluşturur. TPV sistemlerin verimliliği, PV hücrenin bant aralığı enerjisi üzerinde yüksek, altında düşük yayma sağlayan rezonatörlerin yayıcıda kullanımıyla iyileştirilebilir. Daha önce MIM yapıların TPV yayıcı olarak tasarlanma girişimleri olmasına rağmen, farklı rezonatör şekillerinin optimizasyon ve kapsamlı incelenmesi eksiktir. Bu çalışmada, GaSb PV hücre ile eşleştirilmek üzere, W-$SiO_2$-W nanoyapılı geniş bant TPV yayıcılar optimize edilmiştir. Zamanda sonlu farklar yöntemi ve parçacık sürü optimizasyonu kullanılarak, disk, kare, piramit ve koni olmak üzere dört rezonatör şeklinin boyutları, emisivitelerinin GaSb hücrenin kuantum verimliliğiyle spektral olarak eşleşmesi için nümerik olarak optimize edilmiştir. Optimize edilen yayıcılar; verim, güç çıktısı, harcanan malzeme miktarı, yayma açısı ve sıcaklık değişimine karşı optik davranışları bakımından karşılaştırılmıştır. 1600 K yayıcı sıcaklığında, 2.335-2.418 $W \cdot cm^{-2}$ aralığında elektriksel güç çıktısı ve %56.2-57.6 aralığında spektral verim elde edilmiştir. Düz yapılı rezonatörlerin, sivri yapılı rezonatörlerle benzer performanslara, daha alçak boyutta nanoyapılarla ulaştığı gözlenmiştir. İncelenen şekiller arasında, disk rezonatör kullanan yayıcıların en yüksek verime en az malzeme kullanımı ile eriştiği gözlenmiştir. Disk rezonatörlü yayıcının, aynı sıcaklıkta düz W yayıcıya göre, oldukça yüksek spektral verim ve elektriksel güç çıktısı sağlayacağı

gösterilmiştir (sırasıyla, %34 ve %215). Çalışmanın sonuçları, nano elamanların TPV sistemlerde başarılı kullanım ve üretim potansiyelini göstermektedir.

**Anahtar Kelimeler:** Metal-yalıtkan-metal, seçici yayıcı, yüzey plazmon polariton, manyetik polariton, nanoyapı, ısıl radyasyon harmanlaması, parçacık sürü optimizasyonu.

## NOMENCLATURE

| | |
|---|---|
| $E$ | Electric field intensity [V m$^{-1}$] |
| $E_g$ | Bandgap energy [eV] |
| $E_{\lambda,b}$ | Spectral blackbody radiation [W m$^{-2}$ μm$^{-1}$] |
| $E_{in}$ | In-band radiation [W m$^{-2}$] |
| $E_{total}$ | Total emissive power [W m$^{-2}$] |
| $EQE$ | External quantum efficiency |
| $F$ | Objective function |
| $FF$ | Fill factor |
| $J$ | Current density [A m$^{-2}$] |
| $J_0$ | Reverse saturation current density [A cm$^{-2}$] |
| $J_{sc}$ | Short circuit current density [A cm$^{-2}$] |
| $P_{el}$ | Electrical power output [W cm$^{-2}$] |
| $T_E$ | Emitter temperature [K] |
| $T_C$ | TPV cell temperature [K] |
| $V_{oc}$ | Open circuit voltage |
| $c$ | Speed of light in vacuum [$2.998\times10^{8}$ m s$^{-1}$] |
| $d$ | Diameter or base width of the resonator [nm] |
| $h$ | Height of the resonator [nm], Planck's constant [$6.626\times10^{-34}$ m$^2$ kg s$^{-1}$] |
| $k$ | Wave vector [m$^{-1}$] |
| $k_b$ | Boltzmann constant [$8.617\times10^{-5}$ eV K$^{-1}$] |
| $n$ | Ideality factor |
| $t$ | Thickness of the dielectric layer [nm] |
| $q$ | Charge of an electron [$1.602\times10^{-19}$ C] |
| $x$ | Position of the particle |
| $v$ | Velocity of the particle |
| $\Lambda$ | Period of the nanostructure [μm] |
| $\alpha_\lambda$ | Spectral absorptivity |
| $\beta$ | Amendment factor |
| $\varepsilon_\lambda$ | Spectral emissivity |
| $\eta_E$ | Emitter (spectral) efficiency |
| $\eta_{TPV}$ | Thermophotovoltaic system efficiency |
| $\lambda_g$ | Wavelength of radiation corresponding to the bandgap energy of the cell [μm] |
| $v$ | Normalized open circuit voltage |
| $\rho_\lambda$ | Spectral reflectivity |

## INTRODUCTION

The ever-growing need for energy in the world directs researchers to look for alternative ways to convert energy. Thermophotovoltaic (TPV) conversion is among the promising candidates. A TPV system converts infrared radiation emitted by a thermal source (emitter) directly into electrical power by means of a photovoltaic (PV) cell (receiver). Silicon (Si) and Gallium antimonide (GaSb) are among the two most popular PV cells used in TPV prototypes (Ferrari, et al., 2014), while the low bandgap of GaSb ($E_g$ = 0.72 eV) (Adachi, 2013) makes it more suitable compared to Si ($E_g$ = 1.12 eV) for TPV systems with currently attainable emitter temperatures.

The biggest obstacle in development of efficient TPV systems is the spectral mismatch between the thermal emission of the emitter and the PV cell bandgap. An ideal emitter should mainly emit photons with energies higher than or equal to the bandgap of the cell, i.e., in-band photons. TPV system prototypes with GaSb cells usually employ silicon carbide (SiC) or tungsten (W) based emitters (Ferrari, et al., 2014). SiC emitters, although generating a certain amount of power, have very low efficiency due to their high infrared emissivity. W is a suitable selective emitter for GaSb cells since it has high emissivity in the in-band region of the cell. Spectral selectivity can also be achieved by imprinting nanostructures on materials surface. Nanopatterning is usually applied to reduce reflectivity and increase the absorptivity/emissivity of materials (Atak, et al., 2022; Bandiera, et al., 2008; Deinega, et al., 2011; Yüksel, et al., 2015; Sai & Yugami, 2004). Among nanostructured materials, metal-insulator-metal (MIM) configurations were shown to further create multiple plasmonic resonances that allows tunable absorption/emission peaks (Aydın, et al., 2011; Yokoyama, et al., 2016; Lee, et al., 2008; Sakurai, et al., 2015) which exhibits high utility for TPV emitters. A MIM nanostructure is a tri-layer metamaterial consisting of metallic base layer (reflector), a dielectric spacer, and periodically placed metallic patches (resonators) on top. Several researchers employed MIM structures to design selective TPV emitters (Wang & Zhang, 2012; Woolf, et al., 2014; Song, et al., 2016), solar absorbers (Han, et al., 2016; Han, et al., 2017), and TPV cells (Isobe & Hanamura, 2019). MIMs consisting of W and $SiO_2$ were shown to produce broadband and high emissivity/absorptivity in the available region of GaSb related cells. For example, Wang and Zhang (Wang & Zhang, 2012) designed a TPV emitter with W base, $SiO_2$ spacer, and W strips (W-$SiO_2$-W) which showed near unity absorption in the range 0.73-1.83 μm. Zhang, et al. (2021) designed a W-$SiO_2$-W absorber with W strips with trapezoidal profile that showed high absorption between 0.55-1.9 μm. However, the one-dimensional grating structure causes polarization dependence of the emissivity, and resonators as tall as 2300 nm are used. Zhao, et al. (2013) reported a similar emitter design with square resonators, showing polarization independent and high emissivity between 0.7-1.8 μm. Han, et al. (2017) fabricated W-$SiO_2$-W based solar absorber with disk resonators that showed an absorptivity over 90% between 0.5–1.75 μm, which remained unchanged for incidence angles up to 40°. Zhao and Fu (2016), numerically investigated a multilayer periodic $SiO_2$-W-$SiO_2$-W grating and achieved high emissivity suitable for InGaSb cells. The performance of their design is similar to that of MIMs; however, its structure is challenging in terms of fabrication.

Recent W based emitter designs encountered in the literature have room for improvement. A major issue is that the optical properties of W are mostly evaluated at

room temperature and considered in the same way to design selective emitters (Yüksel, et al., 2015; Wang & Zhang, 2012; Song, et al., 2016; Zhao, et al., 2013; Sakurai & Matsuno, 2019; Celanovic, et al., 2008; Blandre, et al., 2019), although the spectral emissivity of W varies greatly with temperature (Touloukian & DeWitt, 1970; Roberts, 1959). Feasible TPV systems should be operated at high temperatures (>1000 K) to generate enough power for use. Temperature dependence of spectral emissivity of W has considerable effect on the efficiency estimation of TPV systems (Atak, 2021). As an exception, the emitter design of Silva-Oelker et al. (2018) does take high temperature optical properties of W into account in their design. However, the one-dimensional periodic structure of the emitter makes the emissivity polarization-dependent and uses W resonators as tall as 1 μm to reduce this dependency. This presents a fabrication challenge, similar to that of Zhang, et al. (2021). The most important issue is that the majority of MIM studies focus on one resonator type, which are usually disks or square patches. There is limited number of MIM studies with pointy resonators such as trapezoids (Zhang, et al., 2021), pyramids (Zheng, et al., 2019) and truncated pyramids (Dang, 2020), but they are not explored and optimized for TPV applications, and their performance is not compared to MIMs with other resonator shapes. In addition to the optical and thermal performance, the amount of material consumption is also affected by the shape of the resonators, which is important for large scale fabrication. Thus, a comprehensive study on the effect of shape on the performance of TPV emitters should be performed.

Considering aforementioned gaps in the literature, the objective of the present study is to optimize W and $SiO_2$ based MIM emitters with differently shaped resonators, to be paired with GaSb cells, and systematically investigate the effect of resonator shape on the emitter performance. The parameter optimized in this work is the shape of the nano-elements, and the evaluation includes the following four homeomorphic resonator shapes: squares, disks, pyramids, and cones. The optimizations are performed to achieve high efficiency and power output at elevated temperatures. The optimized structures are compared in terms of spectral efficiency, power output, TPV system efficiency, material consumption, as well as optical response to the changes in the emission temperature and angles.

## MATERIAL AND METHOD

### Material

In this study, GaSb is selected as the TPV cell material, due to its low bandgap and maturity of systems with GaSb cells. GaSb has a direct bandgap of 0.72 eV (Adachi, 2013) , which corresponds to the energy of a photon at a wavelength of 1.72 μm. According to Wien's Displacement Law, in order to have thermal radiation peak at this wavelength, a blackbody should be heated up to 1680 K. In this work, W is selected as the metal base, due to its high melting temperature (3695 K) and low evaporation rate in vacuum at temperatures up to 2000 K (Gombert, 2003), exhibiting high temperature stability.

In MIM designs, weakly absorbing dielectric oxides are usually used as the dielectric layer. $SiO_2$ is chosen as the dielectric spacer in this work due to its high transmissivity of the light in the visible and near infrared range and high melting temperature (1983 K). MIMs composed of W and $SiO_2$ have been successfully fabricated as TPV emitters (Sakurai & Matsuno, 2019), and solar absorbers (Han, et al., 2017). Kim et al. (2017) has shown that a TPV emitter composed of multiple W and $SiO_2$ thin layers were stable at 1300 K although they displayed delamination spots at 1400 K. Compared to the design of Kim et al. (2017), the MIM structure considered in this work has fewer layers, hence it is expected to be more resistant to delamination at higher working temperatures. In this study, the MIM designs to be optimized are composed of a W substrate, $SiO_2$ dielectric layer, and periodically spaced W resonators on top.

### Method

An ideal broadband TPV emitter has an emissivity of 1 above the bandgap and 0 below the bandgap as given in Eq (1). However, obtaining an emissivity spectrum with a sharp cut-off is challenging, if not impossible. In order to maximize in-band radiation with high utility, researchers usually try to obtain a peak emissivity at around the bandgap.

$$\varepsilon(\lambda) = \begin{cases} 1, & 0 < \lambda \leq \lambda_g \text{ μm} \\ 0, & \lambda > \lambda_g \text{ μm} \end{cases} \quad (1)$$

Having a peak emissivity at $\lambda_g$ results in considerable emission for $\lambda > \lambda_g$, which in turn decreases the overall efficiency. Other than the bandgap, one alternate parameter for TPV emitter design is the external quantum efficiency (*EQE*) of the cell. *EQE* is defined as the number of electron-hole pairs created per incident photon. In PV cell applications, *EQE* peak does not always overlap with the bandgap. For example, GaSb has a bandgap of 1.72 μm, but GaSb cell produced by JX Crystals (JXC) has its peak *EQE* (which is around 80%) centered at $\lambda$ = 1.5 μm and has nonzero values up to 1.80 μm (Fraas, et al., 2002). A selective emitter matching the high *EQE* region would have less out-of-band radiation while maximizing the electrical power output. For wavelengths below 0.6 μm, the *EQE* of GaSb is low and the amount of radiation emitted by TPV emitters at attainable temperatures (1000-2000 K) is negligible. Therefore, the high emissivity region is set as 0.6-1.8 μm. The emissivity for wavelengths longer than 1.8 μm should be suppressed to keep the out-of-band radiation low. With these considerations, an objective function was developed to maximize the emissivity of the emitter within the high external quantum efficiency region of the

GaSb cell while suppressing the out-of-band radiation. The objective function ($F$) is defined in Eq. (2).

$$F = \frac{\int_{0.6}^{1.8} E_{\lambda,b}\varepsilon_\lambda(\lambda)d\lambda}{\int_{0.6}^{1.8} E_{\lambda,b}d\lambda} - \frac{\int_{1.8}^{5} E_{\lambda,b}\varepsilon_\lambda(\lambda)d\lambda}{\int_{1.8}^{5} E_{\lambda,b}d\lambda} \qquad (2)$$

In order to prevent additional emissivity peaks, the long wavelength limit of the low emissivity region is taken as 5 μm. In this context, $F$ is a measure of the selectivity of the emitter, where high in-band emissivity and low out-of-band emissivity maximizes its value. For an ideal emitter, $F$ should be unity. A similar optimization method is previously used in the optimization of MIM emitters for the GaSb cell where the designed emitter showed both higher emitter efficiency and higher in-band radiation than frequently used emitters such as silicon carbide (SiC) and W (Atak, et al., 2021).

In the current design of W-$SiO_2$-W emitter, the bottom W layer is assumed to optically thick, i.e., the transmission through it is assumed zero. By Kirchhoff's law, for a body at equilibrium, the emissivity and the absorptivity should be equal at all wavelengths. Therefore, the spectral emissivity can be calculated using Eq. (3):

$$\varepsilon_\lambda = \alpha_\lambda = 1 - \rho_\lambda \qquad (3)$$

The calculation of reflectivity from nanostructured surfaces requires Maxwell's equations to be solved. For this purpose, a numerical algorithm, the Finite-Difference Time-Domain (FDTD) method is employed. Originally developed by Yee (1996), FDTD aims to solve for the interaction of electromagnetic radiation with arbitrarily complex geometries, by discretizing the Maxwell's curl equations. FDTD method is widely employed in nano-photonics research.

In Figure 1, the four MIM designs and the computational domain of a disk MIM structure are given. A plane light source is incident normal to the $x$-$y$ plane. The $x$ and $y$ boundary conditions are periodic, since the nanostructure design repeats in both directions. The $z$ boundary conditions are set as stretched coordinate perfectly matched layer (PML) in order to prevent reflections from the boundaries. This set of boundary conditions is frequently employed in the simulation of periodic nanostructures (Yüksel, et al., 2015; Sakurai, et al., 2014) and shown to be consistent with experiments (Matsuno & Sakurai, 2017).

In the simulations, optical properties $SiO_2$ are taken from Palik's Handbook (Palik, 1998) since the emissivity of $SiO_2$ is low and shows negligible temperature dependence (Rozenbaum, et al., 1999). The temperature of W is taken to be 1600 K since it was previously shown that W-based TPV emitters can be operated around similar temperatures (Fraas, et al., 2000). In order to account for the change in the emissivity with temperature, the Drude model by Roberts (1959) is used. In order to validate the method, Silva-Oelker et al.'s (2018), W-$HfO_2$-W design with rectangular W strips is studied using FDTD, and the results are compared with those of Silva-Oelker et al. acquired by rigorous coupled-wave analysis (RCWA) method. Silva-Oelker et al.'s (2018) study is chosen for validation since the temperature of W in their design (1680 K) is similar to that of the present study. For accurate results, the mesh step should be at least ten times smaller than the smallest wavelength being simulated (Deinega, et al., 2011). Since wavelengths shorter than 500 nm are not in the scope of this work, the mesh step should be smaller than 50 nm. It is seen that the results converge to a constant value at 5 nm mesh size and decreasing the mesh size further did not improve the results, hence it is used for the rest of the simulations. The result of the present FDTD simulation is compared to the RCWA results of Silva-Oelker et al. (2018). in Figure 2.

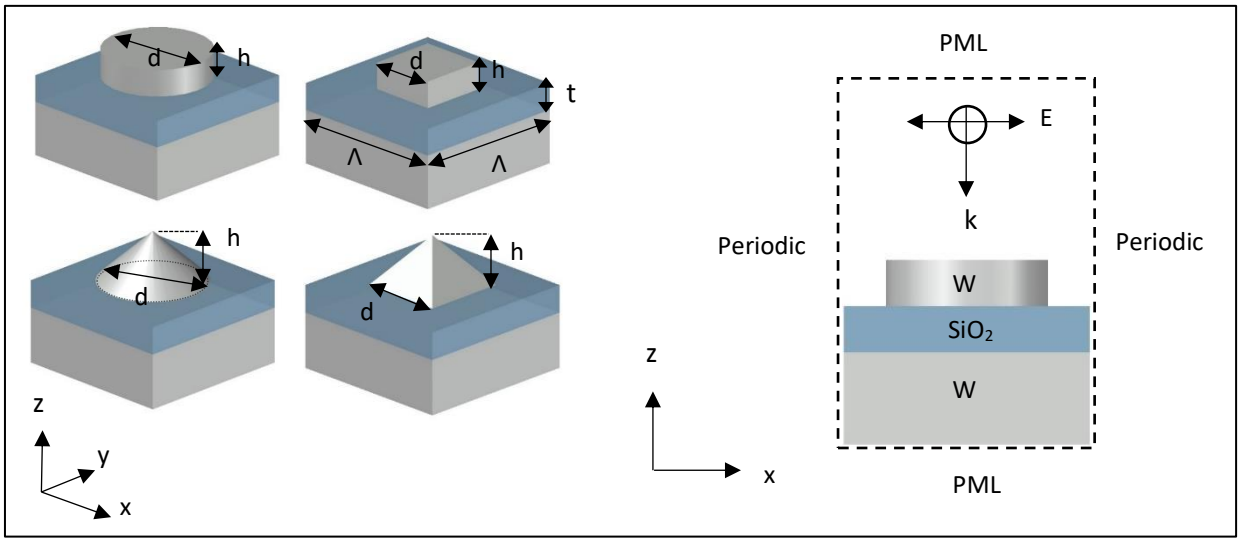


**Figure 1.** The MIM designs and the computational domain of a disk MIM structure.

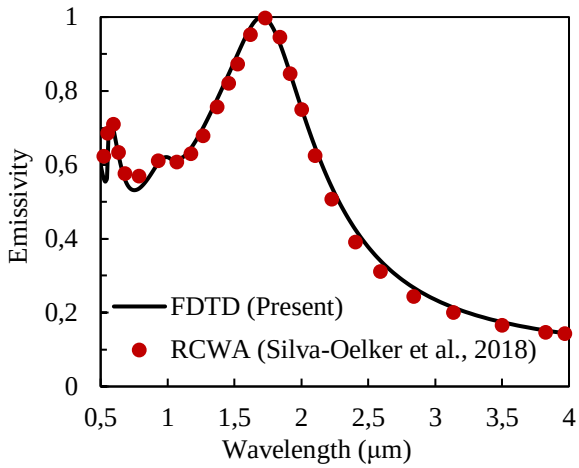


**Figure 2.** Emissivity of W-$HfO_2$-W emitter with rectangular W strips of Silva-Oelker et al. (2018) obtained by RCWA and the present FDTD Simulation

The emissivity spectrum for TM polarized light predicted by FDTD (in the present work) is in good agreement with RCWA results of Silva-Oelker et al. (2018) with a maximum deviation of 9.1%, hence the model is validated.

In another study of W based MIM emitters (Silva-Oelker, et al., 2019), the polarization averaged spectral emissivity is found to be a good approximation of the hemispherical emissivity. Hence, in this study, majority of the FDTD simulations are performed considering normal emissivity.

**Optimization**

The objective function, $F$ defined earlier by Eq. (2) is formed to maximize emitter emissivity within the high external quantum efficiency region of the GaSb cell and suppress the out-of-band radiation. In order to find the nanostructure parameters yielding the highest $F$ given by Eq. (2), Particle Swarm Optimization (PSO) is employed. PSO is a stochastic optimization algorithm designed by Kennedy and Eberhart (1995). In PSO, firstly, possible solutions called "particles" are generated, then these particles are moved in the solution space until maximum number of generations or a given convergence criterion is achieved. The movements of particles are affected both by their personal best positions and the best positions attained by the other particles. A mathematical description of the velocity ($v$) and the position ($x$) of each particle at each iteration are given in Eqs. (5a, 5b) (Shi & Eberhart, 1998). With this iterative process, eventually, all particles are expected to gather around the global best position, similar to bees swarming around the region with highest flower density.

$$v = w \cdot v + c_1 r_1 (p_{best} - x) + c_2 r_2 (g_{best} - x) \quad (5a)$$

$$x = x + v \quad (5b)$$

In Eqs. (5a) and (5b) $w$ is the inertia factor, $c_1$ and $c_2$ are weights, $r_1$ and $r_2$ are random coefficients, $p_{best}$ is the personal best position a particle has encountered, and $g_{best}$ is the global best position encountered by all particles. In this work, $w$ = 0.729 and $c_1$ = $c_2$ = 1.494 are used as recommended by Robinson and Rahmat-Samii (2004) for electromagnetics.

In this optimization scheme, the position ($x$) vector is multidimensional with each dimension representing an optimization parameter. Since each additional parameter increases the computational time exponentially, it is important to assess the impact of each parameter and optimize those with higher impact. The main physical mechanism behind achieving broadband high emissivity with MIM structures is exciting surface plasmon polariton (SPP) and magnetic polariton (MP) resonances close to each other on the spectrum. In Wang and Wang (2013), it was shown that SPP resonance depends on the period, while MP resonance depends on the resonator width. In fact, the cut-off wavelength around 1.8 μm remained unchanged between periods of 0.5-0.8 μm. In other studies, cut-off wavelengths between 1.57-1.83 μm were achieved for periods of 0.5-0.6 μm (Han, et al., 2017; Zhao, et al., 2013; Sakurai & Matsuno, 2019; Khorrami & Fathi, 2019). In a previous study on optimization of W-$SiO_2$-W emitters with periods of 0.4-0.8 μm, it was shown that using 0.4 μm period creates a dip in the emissivity spectra due to the two main resonances being too far apart on the spectrum (Atak, 2021). In the same study, it was also seen that minimum resonator height is obtained at 0.6 μm period. Therefore, in the present work, a period of 0.6 μm is used. Since MP resonance, which determines the cut-off wavelength depends on the resonator width, it is varied between zero and the period for the optimizations performed in this study. The width is equated to base length for square bases and diameter for circular bases. In Wang and Wang (2013), it was observed that the absorptivity in general increases with the resonator height, however, the peak at the MP resonance begins to decrease after 150 nm. In the same study, the thickness of the spacer layer is varied between 30-150 nm. It was seen that the peak absorptivity increased with $SiO_2$ thickness up to 80 nm, beyond which it decreased. In Khorrami and Fathi (2019) it was shown that the emissivity was enhanced gradually by increasing the thickness of the $SiO_2$ layer from 30 nm to 110 nm. Considering these findings, the range of resonator height and $SiO_2$ layer thickness are set to 0-200 nm for the optimization.

In summary, in order to obtain the emissivity profile giving maximum $F$, there are three parameters to be optimized: resonator width ($d$), resonator height ($h$), and the thickness of the dielectric layer ($t$). Within the scope of this study, PSO procedures are followed separately for each shape. The solution space is three dimensional with parameters $t$, $d$, and $h$. For each optimization, 10 random particles are generated initially. These particles are moved through the solution space for 10 generations, and evaluated according to $F$ given in Eq (2).

**Performance Evaluations**

For this study, three metrics are considered to evaluate the performance of TPV systems: the emitter efficiency, the TPV system efficiency (radiation-to-electricity efficiency), and the electrical power output. For the scope of this study, the view factor losses are ignored since emitter and cell are very close and parallel to each other. The performance evaluations are based on the normal emissivity since the emitter and cell usually directly face each other in TPV systems and the selectivity of W-$SiO_2$-W structures is largely independent of angles (Han, et al., 2017). The in-band radiation is defined as the emissive power of the emitter within the wavelength range 0-$\lambda_g$, as in Eq. (6).

$$E_{in} = \int_0^{\lambda_g} \varepsilon_\lambda(\lambda) E_{\lambda,b}(\lambda, T_E) d\lambda \quad (6)$$

The total emissive power radiated from an emitter is defined as in Eq. (7):

$$E_{total} = \int_0^{\infty} \varepsilon_\lambda(\lambda) E_{\lambda,b}(\lambda, T_E) d\lambda \quad (7)$$

The spectral emissive power of a blackbody ($E_{\lambda,b}$) is given by Planck's law (Incropera, et al., 2011) as in Eq. (8):

$$E_{\lambda,b}(\lambda, T_E) = \frac{C_1}{\lambda^5[\exp(C_2/\lambda T_E) - 1]} \quad (8)$$

where $C_1$ = 3.742 × $10^8$ W μm$^4$ m$^{-2}$ and $C_2$ =1.439 × $10^4$ W μm K.

The emitter efficiency ($\eta_E$), also called the spectral efficiency (Fraas, et al., 2003) is defined as the ratio of in-band radiation to the total emissive power of the emitter at a given temperature (Chubb, 2007), and shown in Eq. (9).

$$\eta_E = \frac{E_{in}}{E_{total}} = \frac{\int_0^{\lambda_g} \varepsilon_\lambda(\lambda) E_{\lambda,b}(\lambda, T_E) d\lambda}{\int_0^{\infty} \varepsilon_\lambda(\lambda) E_{\lambda,b}(\lambda, T_E) d\lambda} \quad (9)$$

The overall efficiency of the TPV system depends both the emitter and the TPV cell. The TPV system efficiency ($\eta_{TPV}$), as in Eq. (10), can be calculated by dividing the electrical power output to the radiative power of the emitter. It should be noted that this efficiency assumes a view factor of unity.

$$\eta_{TPV} = \frac{P_{el}}{E_{total}} \quad (10)$$

The electrical power output ($P_{el}$) from a TPV cell is a certain fraction (the fill factor, *FF*) of the product of open circuit voltage ($V_{oc}$) and the short circuit current ($J_{sc}$) (Chubb, 2007) as in Eq. (11):

$$P_{el} = FF \cdot J_{sc} \cdot V_{oc} \quad (11)$$

The maximum current occurs when the TPV cell is short circuited. This is called the short circuit current density, $J_{sc}$ (also known as the photocurrent density) and is calculated using Eq. (12) (Cai, et al., 2020).

$$J_{sc} = \frac{q}{hc} \int_0^{\lambda_g} \varepsilon_\lambda(\lambda) \cdot EQE(\lambda) \cdot E_{\lambda,b}(\lambda, T_E) \lambda d\lambda \quad (12)$$

In Eqs. (6), (9) and (12), $\lambda_g$ of GaSb cell is taken to be 1.80 μm, since JXC standard GaSb cells show nonzero *EQE* up to this value, meaning that current is generated even after the known bandgap of GaSb. When there is no current present, maximum possible voltage is achieved. This is called the open circuit voltage ($V_{oc}$) defined in Eq. (13) (Iles, et al., 1996):

$$V_{oc} = \frac{nk_B T_c}{q} ln \frac{J_{sc}}{J_0} \quad (13)$$

In Eq. (13), *n* is the ideality factor that is assumed to be 1. The reverse saturation current density ($J_0$), also known as the dark current, is the current flowing when there is no light present. $J_0$ depends on the material as well as the temperature of the cell. In the case of GaSb cell, an expression for $J_0$ in units A/cm$^2$ is derived by Fraas et al. (1991) as in Eq. (14):

$$J_0 = 1.84 \cdot 10^{-3} T_c^3 \exp\left(\frac{-E_g}{k_B T_c}\right) \quad (14)$$

Then, the fill factor (Eq. (15)) is calculated by (Qiu, et al., 2006):

$$FF = \beta \frac{\nu - \ln(\nu + 0.72)}{\nu + 1} \quad (15)$$

where $\nu$ is the normalized open circuit voltage given as in Eq. (16) (Iles, et al., 1996):

$$\nu = \frac{V_{oc}}{nk_B T_c / q} \quad (16)$$

In Eq. (15), $\beta$ is the amendment factor which accounts for cell parasitic losses. In the present work, $\beta$ = 0.96 is used as recommended by Qiu et al. (2006). In Eqs. (13), (14) and (16), the cell temperature ($T_c$) is assumed to be 300 K. In Eqs. (6), (9) and (12), considering the JXC standard GaSb cells, $\lambda_g$ is taken as 1.8 μm in order to accurately calculate the power.

**RESULTS AND DISCUSSION**

The optimum parameters found by PSO, the volumes of the resonators and the corresponding *F* values are presented in Table 1. All of the emitters converged to similar values of *F*, with almost identical $SiO_2$ thicknesses. However, the volume of the resonator varied from shape to shape. Cone and pyramid resonators tend to have smaller widths while having greater heights compared to disk and square ones.

**Table 1.** The optimized nanostructure parameters and corresponding values of objective function, *F*

| Resonator Shape | $SiO_2$ Thickness (nm) | Resonator Height (nm) | Resonator Width (nm) | Resonator Volume ($nm^3$) | *F* |
|---|---|---|---|---|---|
| Disk | 112 | 28 | 322 | $2.28\times10^6$ | 0.714 |
| Square | 113 | 36 | 276 | $2.74\times10^6$ | 0.715 |
| Cone | 113 | 93 | 344 | $2.88\times10^6$ | 0.710 |
| Pyramid | 113 | 105 | 285 | $2.84\times10^6$ | 0.711 |

The smallest resonator height and volume are obtained with the disk resonator. The height of the disk resonator is 28 nm which is smaller than the resonators of similar W based MIM emitters/absorbers (Wang & Zhang, 2012; Song, et al., 2016; Han, et al., 2016; Han, et al., 2017; Zhao, et al., 2013; Sakurai & Matsuno, 2019; Silva-Oelker, et al., 2018; Wang & Wang, 2013; Khorrami & Fathi, 2019). It is seen that cone and pyramid structures tend to become taller compared to disk and square, in order to achieve similar *F*. Among the four shapes, pyramid is the tallest with 105 nm height. which is still much smaller compared to a similar W-$SiO_2$-W design with trapezoidal resonators (Zhang, et al., 2021).

In Figure 3, spectral emissivity of optimized MIM emitters with the four resonator shapes are shown in addition to the spectral emissivity of plane W at 1600 K and *EQE* of GaSb (Fraas, et al., 2002) . It is seen that MIM emitters regardless of the resonator shape can be optimized to demonstrate high spectral selectivity. Compared to plain W emitter, W-$SiO_2$-W configurations have substantially higher emissivity in the in-band region, whereas emissivity becomes almost identical to that of plain W around 5 μm. All four emitters showed emissivity peaks at similar wavelengths, two peaks at 0.64 μm, 0.78 μm and a third peak between 1.22-1.28 μm.

Although the emitters are optimized to be used at 1600 K, it is useful to see how their selectivity is affected by temperature. In Figure 4, the emissivity spectra of W-$SiO_2$-W emitters at temperatures of 300 K, 1100 K, and 1600 K are shown. The optical properties of W at room temperature were taken from Palik's Handbook (Palik, 1998) while Drude model of Roberts (1959) is used for higher temperature considerations. It is seen that the locations of emissivity two leftmost peaks around are the same at all temperatures, however the rightmost peak shifts towards lower wavelengths with increasing temperature. The shift of the third peak between 300 K and 1600 K temperatures is about 440-460 nm for disk, square and cone resonators, and 360 nm for the pyramid. It can be said that the selectivity of pyramid resonators is less prone to changes in the temperature compared to other shapes.

Next, the change in the emissivity spectra with the angle of emission (the angle between emission and the surface normal) is investigated. In Figure 5, the emissivity spectra of the selective emitter at different angles are shown. The angular emissivity values are calculated by averaging TM and TE polarizations. It can be seen that all emitters preserve high selectivity at the angle of emission 30°. Although the emissivity at the leftmost two peaks decreases with the increasing angle, the third peak remains relatively unchanged. This can be explained by the excitation of MP around this wavelength. It should be noted that the rightmost peak of the cone emitter undergoes a slight shift towards higher wavelengths at 30°, dissimilar to the others.

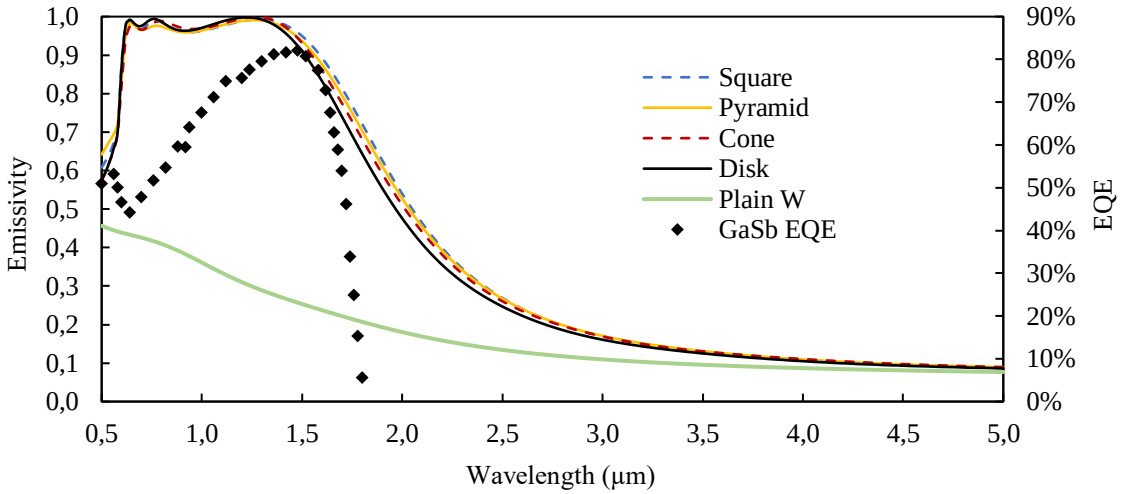


**Figure 3.** Comparison of the emissivity spectra of MIM emitters with different shapes, and plain W at 1600 K

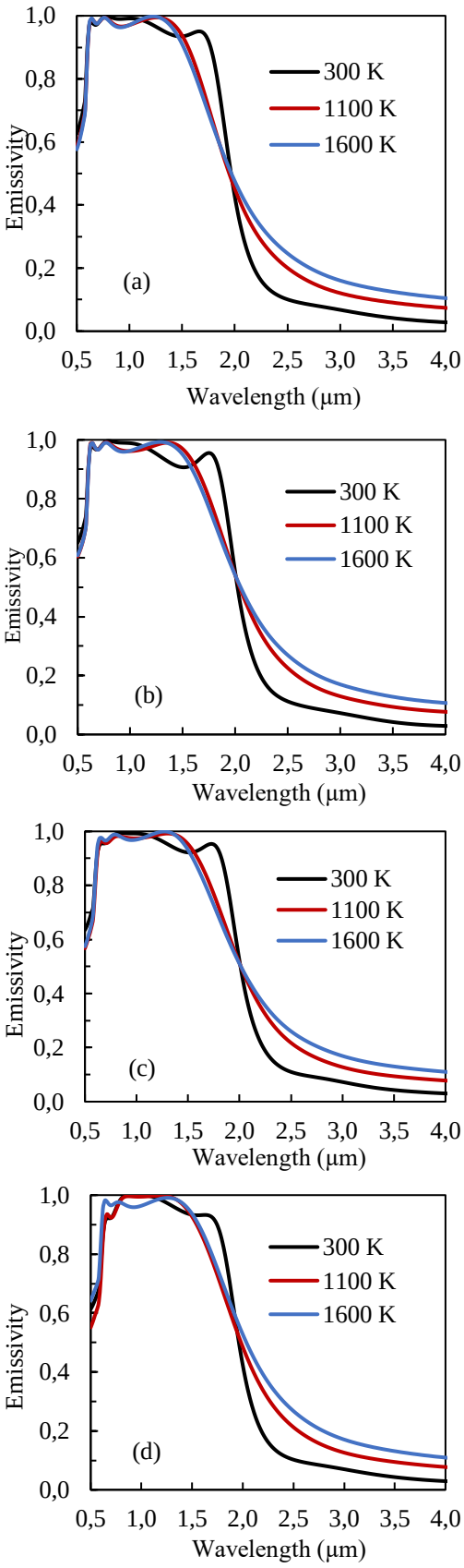


**Figure 4.** The emissivity spectra of optimized W-$SiO_2$-W emitters with disk (a), square (b), cone (c), and pyramid (d) resonators at different temperatures

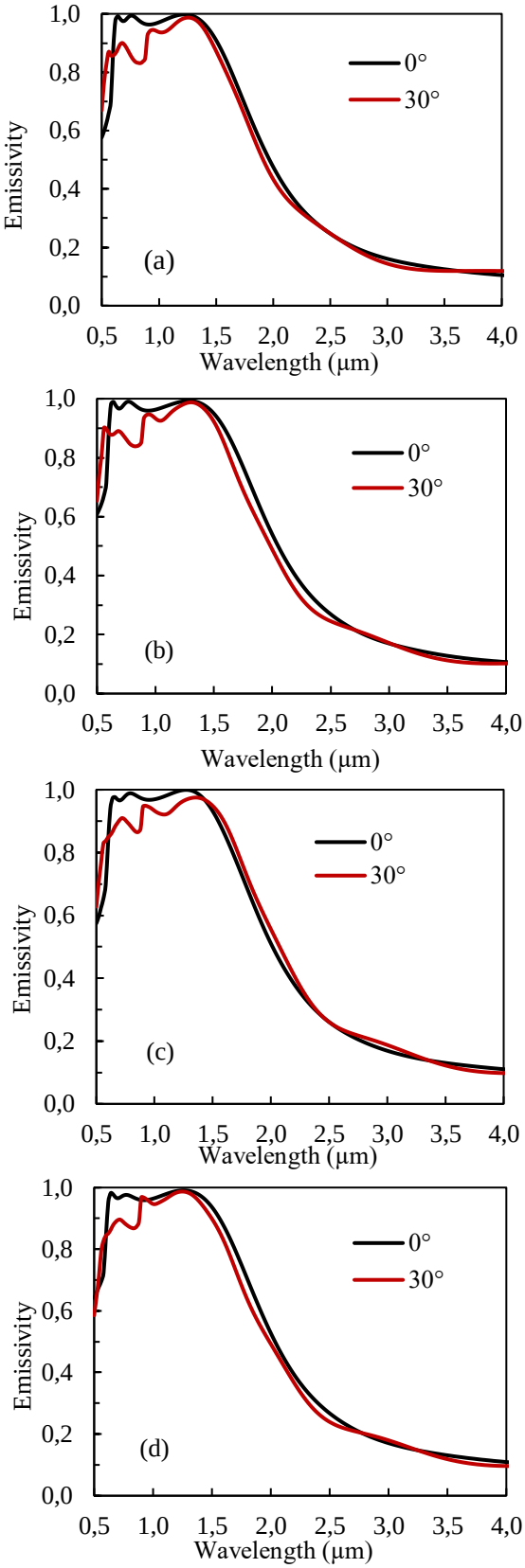


**Figure 5.** Spectral emissivity of the MIM emitter at different emission angles, for disk (a), square (b), cone (c), and pyramid (d) resonators

**Table 2.** The spectral efficiency, TPV efficiency and power output for the investigated emitters at 1600 K paired with GaSb cells. The top four rows list the optimized emitters of the present study.

| Emitter | $\eta_E$ | $P_{el}$ (W cm$^{-2}$) | $\eta_{TPV}$ |
|---|---|---|---|
| Disk MIM | 57.62% | 2.335 | 16.53% |
| Square MIM | 56.31% | 2.418 | 16.18% |
| Cone MIM | 56.63% | 2.381 | 16.26% |
| Pyramid MIM | 56.23% | 2.392 | 16.14% |
| Plain W | 42.93% | 0.741 | 11.20% |
| Blackbody | 24.58% | 2.605 | 7.01% |
| Ideal Emitter | 100.00% | 2.605 | 28.53% |

Considering normal emissivity spectra, the emitter efficiency, TPV efficiency and power output are presented in Table 2 for optimized MIM and other emitters at 1600 K paired with GaSb cells. The emissivity spectrum of the ideal emitter is given by Eq. (1) with $\lambda_g$ taken as 1.8 μm to cover all the wavelengths with nonzero quantum efficiency. It is observed that on average, $\eta_{TPV}$ is less than 30% of $\eta_E$, which means that most of the in-band radiation does not contribute to the electrical power. This loss can be attributed to thermalization, surface recombination, and other intrinsic cell losses. The highest TPV efficiency is obtained with the disk resonator, while the highest power output is obtained from square resonator. The difference in efficiency and power output results can be explained by the difference in emissivity after the third peak towards the out of band region as observed from Figure 3. Compared to the planar W emitter at the same temperature, the MIM emitter with disk resonator demonstrates 215.1% higher power and 34.2% higher spectral efficiency.

Although the efficiency and power outputs are similar, the disk resonator can be argued to be the most advantageous in terms of fabrication. Since it has the shortest height among others, its top-down fabrication requires less material and has shorter sputtering time. The volume of the disk is 17% smaller compared to the square resonator which is closest to disks resonator in terms of volume. That means it is also advantageous in terms of bottom-up fabrication. Therefore, we consider the configuration with the disk resonator for further investigations.

In Figure 6, considering temperature dependent emissivity, the efficiency of the TPV system with GaSb cell and optimized disk emitter is presented compared to the ideal and the blackbody emitters in the temperature range 1000 - 1800 K. For validation, the efficiency of a TPV system with blackbody emitter and JXC GaSb cell calculated by Sakurai and Matsuno (2019) is presented as well. It is seen that the efficiency of the optimized emitter is 2-6 times of that of the blackbody emitter and within 24-65% of the ideal emitter.

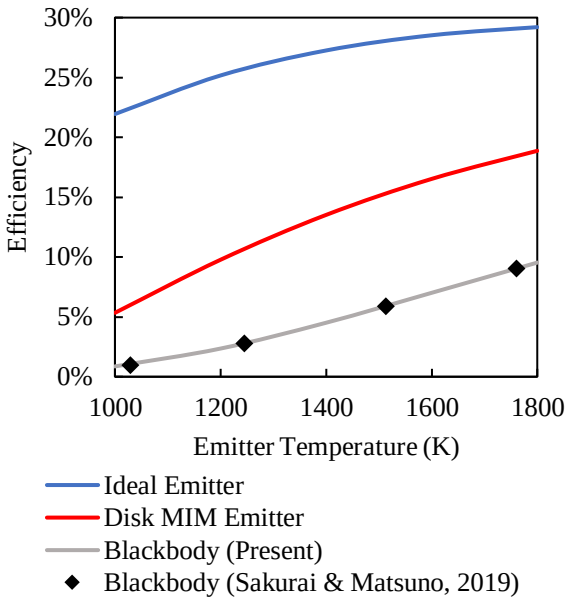


**Figure 6.** TPV system efficiencies for the MIM emitter, the ideal emitter, and the blackbody emitter in the range 1000 - 1800 K.

The efficiency values obtained by ideal, selective, and blackbody emitters tend to get closer as the temperature increases. This can be explained by the shifting of the peak emissive power towards lower wavelengths according to Wien's Displacement Law. With increased temperature, the ratio of in-band radiation to the total emissive power increases for all emitters considered. It should be noted that the ideal emitter in this context does not represent the ultimate attainable efficiency with a predetermined cell, rather, it represents maximum attainable efficiency while keeping the power output at maximum. In Figure 7, the power outputs at different emitter temperatures are presented for the selective emitter and blackbody emitter. Between emitter temperatures of 1000-1800 K, the emitter optimized in this study has a power output of 0.043-5.261 W cm$^{-2}$ that is about 87-90% of that of a blackbody.

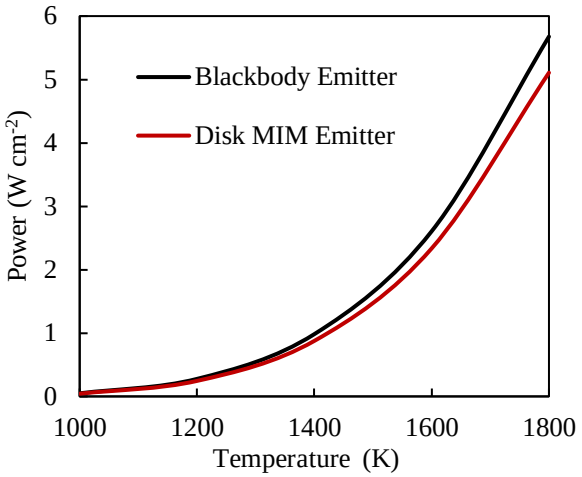


**Figure 7.** Electrical power outputs from TPV systems with the selective emitter and blackbody at different temperatures

## CONCLUSIONS

In this study, an improved selective emitter design is proposed in order to work optimally with a standard GaSb TPV cell. MIM emitters based on W-$SiO_2$-W structure with different resonator shapes are optimized and their performances are compared. The nanostructures considered in this work are disks, squares, cones, and pyramids. During the design of the MIM selective emitter, first, an objective function was developed to maximize the emissivity of emitter within the high external quantum efficiency region of the GaSb cell while suppressing out-of-band radiation. By using this objective function with the FDTD method and PSO algorithm, the resonator width, height and the thickness of the $SiO_2$ layer of the W-$SiO_2$-W emitters with four different resonator shapes are optimized. The performance of each emitter is compared by their spectral efficiency, TPV system efficiency, power output, material consumption, as well as the optical response to changes in temperature and emission angle. As a result of the optimization, the $SiO_2$ thicknesses converged to almost the same value for all emitters, however the dimensions of W resonators varied depending on the shape. Increasing the temperature is shown to cause the shifting of the cut-off wavelength towards lower wavelengths, with the selectivity of pyramid being affected the least. Increasing the angle of emission is shown to decrease the emissivity at short wavelengths but it does not change the emissivity peak near the cut-off wavelength, with the exception of cone resonators. However, the differences in the response of resonators to the angle and temperature effects are not significant enough to reach robust conclusions. At 1600 K, with normal emissivity, spectral efficiencies between 56.23-57.62% and electrical power outputs of 2.335-2.418 W $cm^{-2}$ are obtained. Since the emissivity of MIM structures are minimally affected by the emission angles, hemispherical emissivity is expected to be similar to that of normal emissivity. Although the performances are similar, it was found that the flat type of resonators have smaller heights and volumes compared to pointy resonators, making them preferable for fabrication. Among all designed emitters, the disk emitter is found to be the most efficient while having the smallest volume, hence material consumption. At 1600 K, the MIM emitter with disk resonators demonstrated 57.62% spectral efficiency and 2.335 W $cm^{-2}$ power output, that is 34% more efficient and produces 215% more electrical power compared to plain W emitter at the same temperature. The findings of this work may provide insights on the development and fabrication of efficient selective TPV emitters and solar absorbers which are expected to operate at high temperatures.

## ACKNOWLEDGEMENTS

The first author's graduate education was partially supported by the Scientific and Technological Research Council of Turkey (TUBITAK) through 2210-C National MSc/MA Scholarship Program in the Priority Fields in Science and Technology.

## REFERENCES

Adachi, S., 2013, *Optical constants of crystalline and amorphous semiconductors: numerical data and graphical information*, Springer Science and Business Media.

Atak, E. E., 2021, *Investigation of Nanostructured Surfaces for Thermophotovoltaic Applications*, Master's Thesis, Middle East Technical University, Ankara, Turkey.

Atak, E. E., Elçioğlu, E. B. and Okutucu-Özyurt, T., 2020, Nanostructured silicon design for effectively capturing infrared radiation for near-field TPV applications. *NanoRad 2020 4th International Workshop on Nano-Micro Thermal Radiation*, Shanghai, China.

Atak, E. E., Okutucu-Özyurt, T. and Elçioğlu, E. B., 2021, Metal-Insulator-Metal Selective Emitter Design with an Emissivity Matching with Gasb Thermophotovoltaic Cell. *Proceedings of CHT-21 ICHMT International Symposium on Advances in Computational Heat Transfer*. Begel House Inc.

Aydın, K., Ferry, V. E., Briggs, R. M. and Atwater, H. A., 2011, Broadband polarization-independent resonant light absorption using ultrathin plasmonic super absorbers. *Nature communications*, 2(1), pp. 1-7.

Bandiera, S., Jacob, D., Muller, T., Marquier, F. Laroche, M.; Greffet, J. J., 2008, Enhanced absorption by nanostructured silicon. *Applied Physics Letters*, 93(19).

Blandre, E., Vaillon, R. and Drévillon, J., 2019. New insights into the thermal behavior and management of thermophotovoltaic systems. *Optics Express*, 27(25).

Cai, Q., Chen, P., Cao, S., Ye, Q., Wu, X., 2020, Performance Analysis of GaSb Cell and Thermophotovoltaic System Under Near-Field Thermal Radiation. *International Journal of Thermophysics,* 41(12), pp. 1-15.

Celanovic, I., Jovanovic, N. and Kassakian, J., 2008, Two-dimensional tungsten photonic crystals as selective thermal emitters. *Applied Physics Letters,* 92(15).

Chubb, D., 2007, *Fundamentals of thermophotovoltaic energy conversion*, Elsevier, Amsterdam, The Netherlands.

Dang, P. T., 2020, Efficient broadband truncated-pyramid-based metamaterial absorber in the visible and near-infrared regions. *Crystals,* 10(9), p. 784.

Deinega, A., Valuev, I., Potapkin, B. and Lozovik, Y., 2011, Minimizing light reflection from dielectric textured surfaces. *JOSA A,* 28(5), pp. 770-777.

Ferrari, C., Melino, F., Pinelli, M., Spina, P. R., Venturini, M., 2014, Overview and status of thermophotovoltaic systems. *Energy Procedia,* Volume 45, pp. 160-169.

Fraas, L. M., Avery, J. E., Gruenbaum, P. E., Sundaram, V. S., Emery, K., Matson, R., 1991, Fundamental characterization studies of GaSb solar cells, In *Conference Record of the Twenty-Second IEEE Photovoltaic Specialists Conference-1991.* pp. 80-84.

Fraas, L. M., Avery, J. E., Huang, H. X. and Martinelli, R. U., 2003, Thermophotovoltaic system configurations and spectral control. *Semiconductor Science and Technology,* 18(5), p. S165.

Fraas, L. M., Avery, J. E. and Nakamura, T., 2002, Electricity from concentrated solar IR in solar lighting applications, In *Conference Record of the Twenty-Ninth IEEE Photovoltaic Specialists Conference*, pp. 963-966.

Fraas, L., Samaras, J., Avery, J. and Minkin, L., 2000, *Antireflection coated refractory metal matched emitters for use with GaSb thermophotovoltaic generators.* pp. 1020-1023.

Gombert, A., 2003, An overview of TPV emitter technologies. *AIP conference proceedings,* 653(1), pp. 123-131.

Han, S., Shin, J., Jung, P., Lee, H., Lee, B. J., 2016, Broadband Solar Thermal Absorber Based on Optical Metamaterials for High-Temperature Applications. *Advanced Optical Materials,* 4(8), pp. 1265-1273.

Han, X., He, K., He, Z. and Zhang, Z., 2017, Tungsten-based highly selective solar absorber using simple nanodisk array. *Optics express,* 25(24), pp. A1072-A1078.

Iles, P. A., Chu, C. and Linder, E., 1996, The influence of bandgap on TPV converter efficiency. *AIP Conference Proceedings,* February, 358(1), pp. 446-457.

Incropera, F. P., Lavine, A. S., Bergman, T. L. and DeWitt, D. P., 2011, *Fundamentals of heat and mass transfer,* New York, Wiley.

Isobe, K. and Hanamura, K., 2019, Selective absorption of a thermophotovoltaic cell using a thin semiconductor and a top fishnet-structured electrode. *International Journal of Heat and Mass Transfer,* Issue 134, pp. 807-814.

Kennedy, J. and Eberhart, R., 1995, Particle swarm optimization, in *Proceedings of ICNN'95-international conference on neural networks*. Vol. 4, pp. 1942-1948, IEEE.

Khorrami, Y. and Fathi, D., 2019, Broadband thermophotovoltaic emitter using magnetic polaritons based on optimized one-and two-dimensional multilayer structures. *JOSA B,* 36(3), pp. 662-666.

Kim, J. H., Jung, S. M. and Shin, M. W., 2017, High-temperature degradation of one-dimensional metallodielectric (W/SiO2) photonic crystal as selective thermal emitter for thermophotovoltaic system. *Optical Materials,* Issue 72, pp. 45-51.

Lee, B. J., Wang, L. P. and Zhang, Z. M., 2008, Coherent thermal emission by excitation of magnetic polaritons between periodic strips and a metallic film. *Optics Express,* 16(15), pp. 11328-11336.

Matsuno, Y. and Sakurai, A., 2017, Perfect infrared absorber and emitter based on a large-area metasurface. *Optical Materials Express,* 7(2), pp. 618-626.

Palik, E. D., 1998, *Handbook of optical constants of solids.* Academic press.

Qiu, K., Hayden, A. C. S., Mauk, M. G. and Sulima, O. V., 2006, Generation of electricity using InGaAsSb and GaSb TPV cells in combustion-driven radiant sources. *Solar energy materials and solar cells,* 90(1), pp. 68-81.

Roberts, S., 1959. Optical properties of nickel and tungsten and their interpretation according to Drude's formula. *Physical Review,* 114(1), p. 104.

Robinson, J. and Rahmat-Samii, Y., 2004. Particle swarm optimization in electromagnetics. *IEEE*

*transactions on antennas and propagation,* 52(2), pp. 397-407.

Rozenbaum, O., Meneses, D. D. S., Auger, Y., Chermanne, S., Echegut, P., 1999, A spectroscopic method to measure the spectral emissivity of semi-transparent materials up to high temperature. *Review of scientific instruments,* 70(10), pp. 4020-4025.

Sai, H. and Yugami, H., 2004, Thermophotovoltaic generation with selective radiators based on tungsten surface gratings. *Applied Physics Letters,* 85(16).

Sakurai, A. and Matsuno, Y., 2019, Design and fabrication of a wavelength-selective near-infrared metasurface emitter for a thermophotovoltaic system. *Micromachines,* 10(2), p. 157.

Sakurai, A., Zhao, B. and Zhang, Z. M., 2014, Resonant frequency and bandwidth of metamaterial emitters and absorbers predicted by an RLC circuit model. *Journal of Quantitative Spectroscopy and Radiative Transfer,* Volume 149, pp. 33-40.

Sakurai, A., Zhao, B. and Zhang, Z. M., 2015, Effect of polarization on dual-band infrared metamaterial emitters or absorbers. *Journal of Quantitative Spectroscopy and Radiative Transfer,* Issue 158, pp. 111-118.

Shi, Y. and Eberhart, R., 1998, A modified particle swarm optimizer. In *1998 IEEE international conference on evolutionary computation proceedings. IEEE world congress on computational intelligence* (Cat. No. 98TH8360) pp. 69-73, IEEE.

Silva-Oelker, G., Jerez-Hanckes, C. and Fay, P., 2018, Study of W/HfO 2 grating selective thermal emitters for thermophotovoltaic applications. *Optics express,* 26(22).

Silva-Oelker, G., Jerez-Hanckes, C. and Fay, P., 2019, High-temperature tungsten-hafnia optimized selective thermal emitters for thermophotovoltaic applications. *Journal of Quantitative Spectroscopy and Radiative Transfer,* Volume 231, pp. 61-68.

Song, J., Si, M., Cheng, Q. and Luo, Z., 2016, Two-dimensional trilayer grating with a metal/insulator/metal structure as a thermophotovoltaic emitter. *Applied optics,* 55(6), pp. 1284-1290.

Touloukian, Y. S. and DeWitt, D. P., 1970, *Thermophysical Properties of Matter-The TPRC Data Series. Volume 7. Thermal Radiative Properties-Metallic Elements and Alloys.* New York, Springer.

Wang, H. and Wang, L., 2013, Perfect selective metamaterial solar absorbers. *Optics express,* 21(106), pp. A1078-A1093.

Wang, L. P. and Zhang, Z. M., 2012, Wavelength-selective and diffuse emitter enhanced by magnetic polaritons for thermophotovoltaics. *Applied Physics Letters,* 100(6), p. 063902.

Woolf, D., Hensley, J., Cederberg, J. G., Bethke, D. T., Grine, A. D., Shaner, E. A., 2014, Heterogeneous metasurface for high temperature selective emission. *Applied Physics Letters,* 105(8), p. 081110.

Yee, K., 1966, Numerical solution of initial boundary value problems involving Maxwell's equations in isotropic media, *IEEE Transactions on antennas and propagation,* 14(3), pp. 302-307.

Yokoyama, T., Dao, T. D., Chen, K., Ishii, S., Sugavaneshwar, R. P., Kitajima, M., Nagao, T., 2016, Spectrally Selective Mid-Infrared Thermal Emission from Molybdenum Plasmonic Metamaterial Operated up to 1000° C. *Advanced Optical Materials,* 4(12), pp. 1987-1992.

Yüksel, A., Heltzel, A. and R.Howell, J., 2015, Design and Optimization of Thermal Selective Emitters for High-Efficiency Thermophotovoltaic (TPV) Power Generation. In *Energy Sustainability, Vol. 56840, p. V001T10A003).* American Society of Mechanical Engineers. San Diego.

Zhang, W. W., Qi, H., Yin, Y. M. and Ren, Y. T., 2021, Tailoring radiative properties of a complex trapezoidal grating solar absorber by coupling between SPP and multi-order MP for solar energy harvesting. *Optics Communications,* Volume 479.

Zhao, B., Wang, L., Shuai, Y. and Zhang, Z. M., 2013, Thermophotovoltaic emitters based on a two-dimensional grating/thin-film nanostructure. *International Journal of Heat and Mass Transfer,* Issue 67, pp. 637-645.

Zhao, Y. and Fu, C., 2016, Numerical simulation on the thermal radiative properties of a 2D SiO2/W/SiO2/W layered grating for thermophotovoltaic applications. *Journal of Quantitative Spectroscopy and Radiative Transfer,* Volume 182, pp. 35-44.

Zheng, P., Sujan, K. and Nianqiang, W., 2019, Converting plasmonic light scattering to confined light absorption and creating plexcitons by coupling a gold nano-pyramid array onto a silica–gold film. *Nanoscale horizons,* 4(2), pp. 516-525.